REAL-TIME ABERRATION CORRECTION FOR MEDICAL ULTRASOUND

M. O'Donnell[1] and K.W. Rigby[2]

[1]Biomedical Engineering Department
University of Michigan, Ann Arbor, MI 48109-2099

[2]GE Global Research
One Research Circle, Niskayuna NY 12309

Abstract – To fully realize the potential of ultrasound imaging, large arrays providing full three-dimensional focusing and diffraction limited resolution must be developed. Due to spatial heterogeneities in the sound velocity, however, several key problems limiting overall image quality must be overcome before such arrays will be clinically useful. We have developed phase aberration correction methods for 2-D anisotropic arrays to minimize the effect of sound velocity variation on image quality. Two methods have been tested to estimate phase profiles with a single transmit pulse using signals from speckle generating scatterers. The first employs cross-correlation between all pairs of neighboring elements. In the other, cross-correlation between signals on all elements and the beam sum are used. Both have advantages and disadvantages for real-time implementation. Nevertheless, each can produce robust aberration corrections yielding greatly improved image quality. A scanner with circuitry for real-time aberration correction has been constructed and tested. Results from this system strongly suggest that marked improvement in clinical image quality can be obtained with real-time aberration correction.

INTRODUCTION

Algorithms compensating for non-uniform sound propagation in the human body have been studied for many years [1-18]. One of the simplest, and arguably still one of the most powerful, methods estimates and corrects wavefront arrival time errors at each element in a large aperture, multi-dimensional array. It assumes that the dominant aberration source can be modeled as a thin layer very near the transducer surface, and ignores refraction (thin layer) and interference (layer is close to the transducer surface), both of which can produce wavefront amplitude variation and pulse shape distortion.

Arrival time errors at individual array elements can be estimated using a number of techniques. Here we focus on two methods developed in our labs over the last 18 years. Both use correlation as the basic tool estimating aberrations in the ultrasound wavefront sampled by the imaging array. The first correlates signals between all neighboring elements to estimate relative arrival time errors [1-2]. These differential delays must be unwrapped across the entire array to produce the full arrival time error function. The second correlates individual element signals with the full array receive signal, i.e., the beam sum, producing a direct estimate of the full arrival time error function [17-18]. Each method has pros and cons, as discussed in the next section.

No matter which method is used, the wavefront must be sampled to preserve the spatial scale of the aberration for meaningful arrival time estimates [19-21]. Measured autocorrelation lengths for ultrasound propagating through excised abdominal tissue vary considerably, but can be as small as a few mm [8,22]. The element azimuthal pitch of commercial abdominal one-dimensional arrays is well below this length scale, but the elevational height is much larger. Multi-row probes, in which the elevational aperture is subdivided, are essential for meaningful time delay estimation and correction [19, 20, 23-25].

Finally, no matter what method is used, the quality of the estimated arrival time error depends on the quality of the transmit focus [1, 2, 26]. Since some level of correction will improve transmit focusing, an iterative method is very attractive. Arrival time error estimates are added to the applied delay pattern on both transmit and receive for the next transmit firing in the same direction. Improved estimates of the residual error are then obtained because of the improved transmit focus; the beam forming delays are again updated; and so on.

ARRIVAL TIME ERROR ESTIMATION

Differential time delay errors between neighboring elements can be measured using the phase of the zero lag of the complex cross-correlation function [1-2]. That is,

$$\Delta\tau_{im} = (1/2\pi f)\,\text{phase}\left[\sum_{k=k_0}^{k_1} S_{im}(k)\,S^{*}_{(i-1)m}(k)\right], \quad (1)$$

where f is the ultrasound frequency, S_{im} is the analytic (or complex baseband) signal at element i

on beam m, $S_{(i-1)m}$ is the analytic signal for the neighboring element to i on beam m, and $k = \{k_0, k_1\}$ is the user-defined range segment defining the correlation window. Signals contained in Eq. (1) have already been corrected for geometric arrival time differences. Note that the element indexing scheme implies a 1-D aperture, but it can be easily generalized to handle a multi-dimensional one. Also note that the magnitude of the normalized cross-correlation function (i.e., the correlation coefficient) serves as a quality measure of delay estimates.

Because the correlation coefficient between nearest neighbor signals approaches one in the limit of no aberrations and high spatial sampling of the aperture, the precision of time delay estimates can be quite high. The complete phase aberration profile is calculated by unwrapping these differential measurements across the array for each transmit beam to produce a total profile τ_{im}, where i is the element index and m is the beam index.

One problem with this method, as shown in [2,14], is that calculated differential delays will underestimate true differences between elements when speckle sources are used. The magnitude of the underestimation is directly related to the width of the transmit beam. If the transmit beam is significantly distorted, then the unwrapped phase profile will underestimate the true arrival time function. In addition, if all linear terms are removed, then a residual parabolic term remains. This parabolic error, the result of subtracting calculated beam focusing delays from underestimated propagation delays, introduces a bias in the estimated phase profile.

A second problem with nearest neighbor correlations is propagation of measurement error across the array. Even though the precision of an individual differential measurement between two channels can be quite good, the error can propagate across the aperture as differential delays are integrated to form the complete profile. Methods have been developed, however, to minimize integration errors both for 1-D and 2-D apertures [14, 27-28].

In summary, nearest neighbor correlations yield highly precise differential measurements of arrival time errors using signals from speckle generating objects. Some imprecision is introduced in the unwrap process computing the complete error profile across the aperture. In addition, estimation bias is introduced if the transmit beam is greatly distorted. Iteration of the error profile yields an improved transmit beam at each step. Consequently, iteration minimizes the bias and can produce high quality error profile estimates. The only major concern with this algorithm, assuming proper spatial sampling of the imaging aperture, is the number of iterations required to converge to a stable estimate for extremely distorted wavefronts.

A slight variation on the nearest neighbor method, called the beam sum algorithm, solves some of the problems related to estimation bias at the slight expense of estimation precision. This approach correlates each channel signal to the sum of those signals for a given beam direction, i.e., the beam sum [17-18]. That is,

$$\tau_{im} = (1/2\pi f)\,\mathrm{phase}\left[\sum_{k=k_0}^{k_1} S_{im}(k)\,B_m^*(k)\right] \quad (2)$$

$$\tau_{im} = (1/2\pi f)\,\mathrm{phase}\left[\sum_{k=k_0}^{k_1} S_{im}(k)\left(\sum_{j=1}^{N} S_{jm}^*(k)\right)\right],$$

where B_m is the beam sum for the m^{th} beam and N is the total number of channels contributing to the m^{th} beam. Again, all individual element signals used in Eq. (2) have already been corrected for geometric arrival time differences. Note that by using a common reference signal for all channels, the arrival time function τ_{im} is estimated directly.

The simplicity of a common reference signal is particularly attractive for multi-row probes, where direct estimation eliminates any potential problems with unwrapping across a two-dimensional aperture. In addition, beam sum correlation is less susceptible to a single bad estimate. If data on one channel is corrupted, due to interference or refraction effects for instance, then the error is almost entirely limited to that channel. In contrast, if a differential delay must be unwrapped, then corrupted channels must be eliminated or else the entire arrival time profile can be compromised. Indeed, an undetected single element error can greatly reduce the accuracy of an unwrapped profile. Robust estimation is essential, since estimates are the error signal in a real-time feedback loop controlling time delays.

The primary disadvantage of the beam sum method is reduced precision. As noted above, precision is directly related to the magnitude of the correlation coefficient. Nearest neighbor correlation coefficients routinely approach one, whereas beam sum correlation coefficients can be as low as 0.5 for a multi-row aperture even with ideal beam forming [29]. The correlation with the beam sum is proportional to the sum of the correlations with each channel, since

$$\sum_{k=k_0}^{k_1} S_{im}(k)\,B_m^*(k) = \sum_{j=1}^{N}\sum_{k=k_0}^{k=k_1} S_{jm}^*(k)\,S_{im}(k) \quad . \quad (3)$$

The correlation coefficient between signals from pairs of elements (averaged over a speckle-generating target), however, decreases with element separation, reaching a value close to zero for elements on opposite ends of the imaging aperture [30]. Consequently, the correlation coefficients with the beam sum is less than one for all elements, is maximum at the aperture center, and is minimum at

the aperture edges. Lower correlation coefficients produce less precise estimates.

To overcome the reduced precision of beam sum correlations and the bias of nearest neighbor correlations, we have investigated a number of algorithms combining both estimates [14]. The first step is to set a threshold on the beam sum correlation coefficient. Those elements whose correlation to the beam sum exceeds the threshold will retain this error estimate. Remaining elements will then have their error profiles "filled in" using nearest neighbor correlations. These estimates are unwrapped and adjusted linearly within reference points provided by the beam sum correlation. Note that as the beam sum correlation increases with iteration, the threshold relative to the mean also increases.

Using such a procedure, the advantages of both beam sum correlations and nearest neighbor correlations can be exploited. Retaining only those error estimates from beam sum correlations with high correlation coefficients produces low error variance. These points then serve as references for nearest neighbor correlation estimates, thus restricting the extent to which measurement errors can propagate across the array. Furthermore, the parabolic error due to the wide isonifying beam in nearest neighbor estimates is removed linearly piecewise by reference points from the beam sum correlation.

Time delay error profiles are estimated independently on each beam. For a pure phase screen model, the error profile should be independent of the beam direction. However, due to imperfections in the phase screen model, and the limits on correlation accuracy given finite electronic signal to noise ratio in clinical scans, the arrival time error on a given channel varies with transmit beam direction. Several averaging methods have been developed to smooth arrival time variations at a given element assuming that the total error profile across the imaging aperture varies slowly with beam direction. These algorithms produce robust estimates of the arrival time error at each element of multi-dimensional arrays as a function of beam angle, as detailed in [17-18].

As noted above, all algorithms are applied iteratively, where arrival time estimates in one image frame are used to correct transmit and receive beam forming delays in the next frame; new estimates are obtained using the updated beam forming delays and applied as corrections; and so on. We have observed that for both algorithms, or combinations of the two, the procedure almost always stabilizes within three to four frames.

Since the magnitude of the correlation coefficient between either nearest neighbor signals or the beam sum with elemental signals is greatly reduced outside of the transmit focal region, all correlation measurements are centered around the electronic transmit and elevational lens focus of the transducer. A longer correlation region improves electronic signal to noise ratio and reduces the influence of strong, specular reflectors, but it can reduce the average correlation coefficient from speckle. The best compromise between these competing effects usually dictates a correlation window of 20-50 mm.

ADAPTIVE SCANNER

Over the last 15 years we have built several real-time scanners to test both nearest neighbor and beam sum correlation methods. The preferred algorithm, as noted above, combines both methods. As this time, however, the computational load for a combined approach is prohibitive for real-time scanning. Consequently, the system used for the results presented here implemented only the beam sum algorithm for real-time, frame-to-frame aberration correction.

The adaptive imager uses a GE LOGIQ 700 MR ultrasound system connected through a high bandwidth interface to a Mercury Computer Systems multi-processor computer [18, 31]. Thirty-two signals from the LOGIQ 700's 128 beam forming channels are transmitted in parallel to the input devices of the Mercury System. The sum of the 128 beam forming channels (i.e., the beam sum signal) is transmitted over a separate data path, along with timing and control signals. Channel signals are acquired after beam forming delays have been applied. All signals pass through interface boards to electrically isolate the GE LOGIQ scanner from the Mercury system.

Using these inputs, the Mercury system computes complex correlation functions on each channel in the array. Since only 32 channels are acquired on a given transmit firing, four firings are required for every beam. The outputs of correlation processing across the array are output from the Mercury system to a host computer. The host performs all final averaging across beams, and communicates updated delay coefficients to the LOGIQ scanner.

A complete set of beam forming coefficients is updated about three times per second. The computations required to maintain this rate are large but by no means extraordinary – it is about the same order as that required by real-time delay-and-sum beam forming. Beam forming computations are performed on current clinical scanners using banks of custom integrated circuits. The general purpose system used for the studies reported in the next section, as illustrated in Figure 1, is clearly inefficient compared to a custom-designed ASIC array. This system, however, allows a software-based approach with considerable flexibility in algorithm development and data flow.

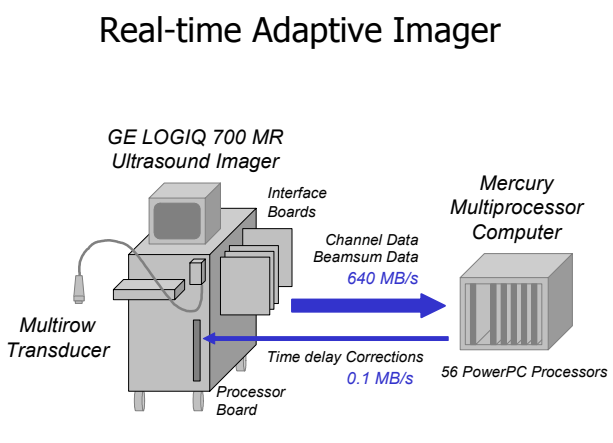

Figure 1. Real-time adaptive imager. A GE LOGIQ 700 MR ultrasound imager sends beam sum and channel data to a Mercury multi-processor computer system. The Mercury system calculates arrival time errors for each beam former channel and sends transmit and receive beam forming time corrections back to the LOGIQ 700.

MULTI-ROW TRANSDUCER

The transducer used for the results reported in the next section contains 576 elements arranged in six elevational rows and 96 azimuthal columns. Each element is 0.6 mm wide and 2.5 mm tall, where the larger dimension is the transducer row (elevational) pitch. Independent electrical connections are provided to each element forming a "1.75-D" array [32]. It operates at a center frequency of 3.35 MHz with about a 75% -6dB fractional bandwidth. The probe has an elevational lens focused at 75 mm.

A linear scan format is used, with each beam formed perpendicular to the transducer face. Beams are translated azimuthally to sweep out the image area. For each beam, 128 elements are connected through multiplexing switches to 128 electronic channels, forming the active aperture for that beam, as illustrated in Figure 2. Although this configuration produces a smaller imaging aperture than typical commercial probes, it is sufficient to test real-time aberration algorithms.

A single transmit focal zone is used. The transmit electronic focus is coincident with the fixed focal length of the elevational lens (75 mm). The spectrum of the transmitted waveform is centered at 3.75 MHz to emphasize higher frequency components within the transducer passband. Dynamic receive focusing is applied in both azimuth and elevation. Note that the nominal geometric focus is symmetric about the aperture center, but arrival time errors are estimated and corrected independently for every element in the 1.75-D array.

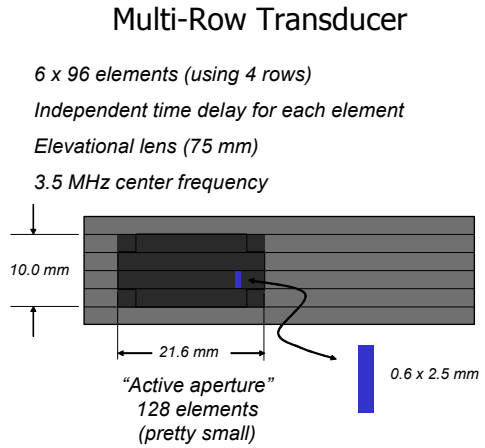

Figure 2. The multi-row transducer has 576 elements arranged in six rows and 96 columns. On each scan line, 128 elements from the four center rows are connected to 128 beam forming channels to form the active aperture (light gray). The active aperture translates across azimuth (i.e., rows) with scan lines forming one image frame.

RESULTS

A large number of clinical scans have been recorded using the system presented in the previous two sections. Two illustrative examples are presented here. All figures consist of an image obtained using the default geometric time delays, an image formed with corrected delays, and a schematic identifying the significant anatomy. Each image pair is presented with the same gain and dynamic range.

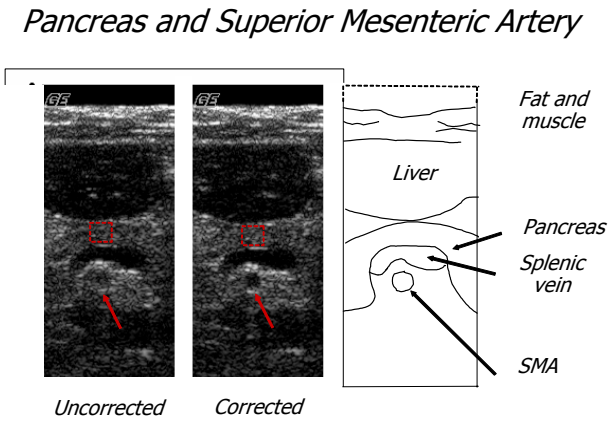

Figure 3. Images of the pancreas before (left) and after (right) correction. The box denotes the transmit and lens focal depth. After correction, the contrast of the superior mesenteric artery (SMA) increases by about 5.8 dB. Note also increased acoustic transmission through the SMA (lower arrow).

The system can continuously update delays on every image frame. An example of a corrected image using this mode is presented in Figure 3, where the two frames were produced about 300 msec apart. For experimental purposes, the machine usually updates beam forming delays for a specific number

of frames, then toggles to default geometric delays for the same number of frames, then updates delays again starting with geometric delays for a specific number of frames, and so on. This mode toggles the display between corrected and uncorrected images to get a visual impression of changes in image quality. Two frames from a long loop recorded while imaging the liver in this way are presented in Figure 4.

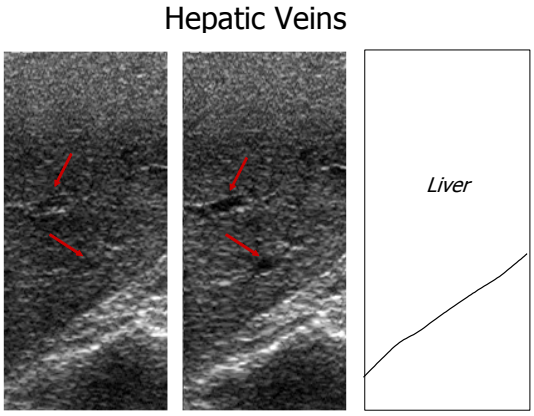

Figure 4. The visibility of these small (approximately 5 mm diameter) blood vessels in the liver improves dramatically after time delay correction (right) compared to the uncorrected image (left).

Observed image improvements are not just a result of adjusting the effective speed of sound, since the algorithm tends to suppress geometric arrival time errors in the azimuthal direction. We have not quantitatively analyzed all error patterns from the large number of clinical scans recorded to date. Based on the small number of scans fully characterized, however, it appears that observable image quality improvements are produced in clinical images when arrival time errors of magnitude less than a wavelength and spatial scale of at least a few mm are corrected.

DISCUSSION

Correlation-based aberration correction can account for beam forming errors in clinical images if distortions due to an inhomogeneous velocity profile can be modeled as a phase screen. We have observed significant improvements in abdominal imaging with a 1.75-D probe using real-time phase aberration correction, suggesting that the phase screen assumption may be reasonable for a large number of clinical scans.

Image quality improvements include increased visibility of known anatomical structures, decreased clutter within blood vessels and increased brightness of speckle generating objects. The studies reported here used a total imaging aperture far smaller than current commercial probes. With increased computational power, real-time adaption will be possible for much large apertures. Such systems may finally realize the potential of large ultrasound arrays providing full three-dimensional focusing and diffraction limited resolution.

ACKNOWLEDGEMENTS

We thank the General Electric Company, the National Institutes of Health, and the Defense Advanced Research Projects Administration (DARPA) for supporting this work. We also thank all the people at GE-CRD and the University of Michigan who've worked on phase aberration correction with us over the last fifteen years.

REFERENCES

[1] S.W. Flax and M. O'Donnell, "Phase-aberration correction using signals from point reflectors and diffuse scatterers: Basic principles," IEEE Trans. Ultrason. Ferroelect. Freq. Contr., vol. 35, pp. 758-767, 1988.

[2] M. O'Donnell and S.W. Flax, "Phase-aberration correction using signals from point reflectors and diffuse scatterers: Measurements," IEEE Trans. Ultrason. Ferroelect. Freq. Contr., vol. 35, pp. 768-774, 1988.

[3] L.F. Nock, G.E. Trahey, and S. Smith, "Phase-aberration correction in medical ultrasound using speckle brightness as a quality factor," J. Acoust. Soc. Am., vol. 85, pp. 1819-1833, 1989.

[4] D. Rachlin, "Direct estimation of aberrating delays in pulse-echo imaging systems," J. Acoust. Soc. Am., vol. 88, pp. 191-198, 1990.

[5] G.E. Trahey, D. Zhao, J.A. Miglin, and S. Smith, "Experimental results with a real-time adaptive ultrasonic system for viewing through distorting media," IEEE Trans. Ultrason. Ferroelect. Freq. Contr., vol. 37, pp. 418-427, 1990.

[6] B. Steinberg, "A discussion of two wavefront aberration correction procedures," Ultrasonic Imaging, vol. 14, pp. 387-392, 1992.

[7] D.A. Carpenter, D.E. Robinson, P.L. Ho, D.C.C. Martin, and P. Issacs, "Body wall aberration correction in medical ultrasonic images using synthetic-aperture data," in Proc. IEEE Ultrason. Symp., 1993, vol. 2, pp. 1131-1134.

[8] L.M. Hinkelman, D.L. Liu, L.A. Metlay, and R.C. Waag, "Measurements of ultrasonic pulse arrival time and energy level variations produced by propagation through abdominal wall," J. Acoust. Soc. Am., vol. 95, pp. 530-541, 1994.

[9] D.L. Liu and R.C. Waag, "Correction of ultrasonic wavefront distortion using backpropagation and a reference waveform method for time-shift compensation," J.

Acoust. Soc. Am., vol. 96, pp. 649-660, 1994.

[10] D.L. Liu and R.C. Waag, "Time-shift compensation of ultrasonic pulse degradation using least-mean-square error estimates of arrival time," J. Acoust. Soc. Am., vol. 95, pp. 542-555, 1994.

[11] R. Mallart and M. Fink, "Adaptive focusing in scattering media through sound-speed inhomogeneities: The van Cittert-Zernike approach and focusing criterion," J. Acoust. Soc. Am., vol. 96, pp. 3721-3732, 1994.

[12] G.C. Ng, S.S. Worrell, P.D. Freiburger, and G.E. Trahey, "A comparative evaluation of several algorithms for phase aberration correction," IEEE Trans. Ultrason. Ferroelect. Freq. Contr., vol. 41, pp. 631-643, 1994.

[13] S. Krishnan, P.C. Li, and M. O'Donnell, "Adaptive compensation of phase and magnitude aberrations," IEEE Trans. Ultrason. Ferroelect. Freq. Contr., vol. 43, pp. 44-55, 1996.

[14] S. Krishnan, K.W. Rigby, and M. O'Donnell, "Improved estimation of phase aberration profiles," IEEE Trans. Ultrason. Ferroelect. Freq. Contr., vol. 44, pp. 701-713, 1997.

[15] Y. Li, "Phase aberration correction using near-field signal redundancy – Part I: Principles," IEEE Trans. Ultrason. Ferroelect. Freq. Contr., vol. 44, pp. 335-371, 1997.

[16] S. Krishnan, K.W. Rigby, and M. O'Donnell, "Efficient parallel adaptive aberration correction," IEEE Trans. Ultrason. Ferroelect. Freq. Contr., vol. 45, pp. 691-703, 1998.

[17] K.W. Rigby, E.A. Addrawis, C.L. Chalek, B.H. Haider, W.L. Hinrichs, R.A. Hogel, W.M. Leue, M.G. Angle, B.T. McCeathron, S.C. Miller, S.M. Peshman, M.A. Peters, L.J. Thomas, S. Krishnan, and M. O'Donnell, "Realtime Adaptive Imaging", in Proc. IEEE Ultrason. Symp., 1998, vol. 3, pp.1603-1606.

[18] K.W. Rigby, C.L. Chalek, B.H. Haider, R.S. Lewandowski, M. O'Donnell, L.S. Smith, and D.G. Wildes, "Improved in vivo abdominal image quality using real-time estimation and correction of wavefront arrival time errors", in Proc. IEEE Ultrason. Symp., 2000, vol. 3, pp. 1645-1653.

[19] G.E. Trahey, "An evaluation of transducer design and algorithm performance for two dimensional aberration correction," in Proc. IEEE Ultrason. Symp., 1991, vol. 2, pp. 1181-1187.

[20] P.D. Freiburger, D.C. Sullivan, B.H. LeBlanc, S.W. Smith, and G.E. Trahey, "Two dimensional ultrasonic beam distortion in the breast: *In vivo* measurements and effects," Ultrasonic Imaging, vol. 14, pp. 398-414, 1992.

[21] D.L. Liu and R.C. Waag, "A comparison of ultrasonic wavefront distortion and compensation in one-dimensional and two-dimensional apertures," IEEE Trans. Ultrason. Ferroelect. Freq. Contr., vol. 42, pp. 726-733, 1995.

[22] L.M. Hinkelman, T.D. Mast, L.A. Metlay, and R.C. Waag, "The effect of abdominal wall morphology on ultrasonic pulse distortion. Part I: Measurements," J. Acoust. Soc. Am., vol. 104, pp. 3635-3649, 1998.

[23] R. Kanda, Y. Sumino, K. Takamizawa, and H. Sasaki, "An investigation of waveform distortion correction: Correction using averaged phase information and the effect of correction in one and two dimensions," in Proc. IEEE Ultrason. Symp., 1991, pp. 1201-1206.

[24] Y. Sumino and R.C. Waag, "Measurements of ultrasonic pulse arrival time differences produced by abdominal wall specimens," J. Acoust. Soc. Am., vol. 90, pp. 2924-2930, 1991.

[25] Q. Zhu, B.D. Steinberg, and R.L. Anderson, "Wavefront amplitude distortion and image sidelobe levels-Part II: In vivo experiments," IEEE Trans. Ultrason. Ferroelect. Freq. Contr., vol. 40, pp. 754-762, 1993.

[26] D.L. Liu and R.C. Waag, "Estimation and correction of ultrasonic wavefront distortion using pulse-echo data received in a two-dimensional aperture," IEEE Trans. Ultrason. Ferroelect. Freq. Contr., vol. 45, pp. 473-490, 1998.

[27] P.C. Li and M. O'Donnell, "Phase aberration correction on two-dimensional conformal arrays", IEEE Trans. Ultrason. Ferroelect. Freq. Contr., vol. 42, pp. 73-82, 1995.

[28] Y. Miwa, R. Shinomura, S. Umemura, and M. O'Donnell, "Optimum Correlator Arrangement for Two-Directional Phase-Aberration Correction", in Proc. IEEE Ultrason. Symp., 1998, vol. 2, pp. 1607-1610.

[29] K.W. Hollman, K.W. Rigby and M. O'Donnell, "Coherence factor of speckle from a multi-row probe", in Proc. IEEE Ultrason. Symp., 1999, vol. 2, pp. 1257-1260.

[30] R. Mallart and M. Fink, "The can Cittert-Zernicke theorem in pulse echo measurements," J. Acoust. Soc. Am., vol. 90, pp. 2718-2727, 1991.

[31] Mercury Computer Systems, Inc. Chelmsford, MA, USA (www.mc.com).

[32] D.G. Wildes et al, "A multi-row transducer array for adaptive imaging," in Proc. IEEE Ultrason. Symp., 1998, vol. 2, pp. 1831-1834.